Tribology in Industry

RESEARCH

Evaluation of Corrosion Resistance of TiN and CrN Films Coated on SS304 Stainless Steel Using Cathodic Arc Deposition

Vu Van Huy[a,*], Nikolai B. Rodionov[b], Valery A. Karpov[c], Ngo Thanh Binh[a], Doan Thanh Van[a], Nguyen Van Thanh[d]

[a]*Joint Vietnam-Russia Tropical Science and Technology Research Center, Ho Chi Minh, Vietnam,*
[b]*Troitsk Institute of Innovative and Thermonuclear Research, Moscow, Russia,*
[c]*Institute of ecology and evolution A.N. Severtsov of the Russian Academy of Sciences, Moscow, Russia,*
[d]*Center for Optoelectronics – CFOC, Hanoi, Vietnam.*

A B S T R A C T

Monolayer (TiN/Ti) and multilayer films (TiN/Ti; CrN/Ti, TiN/CrN/Ti) with an average thickness of 2300 nm were deposited on SS304 steel using the cathodic arc deposition method. Analysis revealed the presence of numerous macroparticles (peaks) and pinholes (valleys) uniformly distributed across the surface. The monolayer film exhibited superior surface quality compared to the multilayer films but demonstrated poor adhesion to the substrate. X-ray diffraction spectroscopy detected a noticeable shift in the preferred orientation of the deposited film, transitioning from (111) to (200) when employing a multilayer structure. Applying ceramic coatings onto stainless steel induced significant alterations in the potentiodynamic polarization curves of monolayer and multilayer films, resulting in a shift towards more noble potentials and lower corrosion currents than the substrate. Furthermore, the potential passive range expanded when employing multilayer structures based on TiN and CrN.

1. INTRODUCTION

The global population aged 60 and over is expected to reach 2 billion by 2050. This demographic change is causing an increase in health issues like osteoporosis, joint inflammation, and bone fractures, leading to a higher demand for orthopedic implants to replace, support, or rebuild damaged bones or joints. Moreover, recent studies [1-2] have shown a rise in postoperative complications in the orthopedic implant manufacturing sector, including infections, allergies, implant rejection, and toxicity issues caused by the release of metal ions and debris. As a result, ongoing research is focusing on developing new implant materials, with an emphasis on improving the biological compatibility and surface mechanical properties of implants through composite coatings, ceramics, and calcium phosphate [3].

Bone fixation devices are typically fabricated using titanium alloys (Ti6Al4V, Ti6Al7Nb) and stainless steel (304L, 316L). Titanium alloys are renowned for their exceptional corrosion resistance, mechanical compatibility with bones, and biological similarity, making them ideal materials for the orthopedic implant industry. However, the high manufacturing cost of bone plates and screws from titanium alloys poses a challenge to their widespread adoption. In contrast, bone fixation devices made from stainless steel are relatively affordable, rendering them suitable for low-income countries such as Vietnam. Nevertheless, long-term implantation of stainless steel devices is not advisable due to their propensity to rust when exposed to bodily fluids. This corrosion releases toxic metal ions, such as Cr^{3+} and Ni^{2+}, which can cause cytotoxicity, allergies, and implant rejection. Research indicates that approximately 10-15% of the population exhibits adverse reactions to metal ions released from implanted devices, accounting for about 60% of unstable implanted devices [4].

Throughout the preceding fifteen-year period, extensive clinical trials have consistently underscored the remarkable corrosion resistance and favorable biocompatibility associated with Titanium Nitride (TiN) and Chromium Nitride (CrN) coatings deposited using Physical Vapor Deposition (PVD) technology. These coatings have been widely applied in orthopedic trauma due to their exceptional performance characteristics. However, it is crucial to note that these coatings are susceptible to forming defects, including pinholes, droplets, and columnar growth. These defects expose the underlying substrate to electrolytes, resulting in reduced corrosion protection, the release of metal ions, film delamination, and the generation of wear debris. One extensively researched solution to address these inherent challenges is the utilization of multilayered coating systems. These advanced systems facilitate re-nucleation, create multiple interfaces, and reduce porosity, thereby impeding micro-crack propagation and preventing the formation of pinholes and pore continuity. Consequently, this approach significantly enhances the polarization resistance of the coatings and reduces their electrochemical porosity, further enhancing their overall performance and durability in orthopedic trauma applications [5,6].

The research conducted by M. Ben Daia et al. [7] focused on the fabrication of Ti/TiN multilayer films consisting of multiple sub-layers (Ti+TiN) with varying period thicknesses ranging from 2.5 nm to 20 nm. These films were produced through reactive sputtering on a silicon substrate. The study revealed an increase in the hardness of the composite layer as the period thickness decreased, with the maximum hardness observed at a period thickness of 2.5 nm. In a separate investigation by N.D. Nam et al. [8], various multilayer films, including Ti/TiN, Cr/TiN, Ti/CrN, and Cr/CrN, were manufactured using RF reactive sputtering on a 316L stainless steel substrate, maintaining sub-layer ratios at 3:7. Notably, the Cr/CrN film demonstrated the highest corrosion protection efficiency, reaching an impressive 99.99%. Q. Yang et al. [9] conducted a study involving the deposition of Ti/CrN/TiN films onto a Ti-6Al-4V titanium alloy substrate through DC magnetron sputtering. X-ray diffraction analysis revealed that the film grew along two primary orientations: (111) and (200). It was observed that films with a preferred orientation of (200) displayed superior hardness.

Meanwhile, M. Herranen et al. [10] studied fabricating Ti/TiN multilayer films using ion-plating techniques. Their findings suggested that increasing the thickness of sub-layers in the coating led to a concurrent enhancement in corrosion resistance. Furthermore, additional studies [11,12] have corroborated these findings and emphasized the augmentation of both mechanical properties and corrosion resistance in Ti/TiN multilayer composite structures. A particularly noteworthy observation was that the interleaving of Ti layers within these structures effectively countered the formation of columnar structures in the TiN film [13,14].

As a result, researching and developing multilayer coatings is a promising direction for enhancing corrosion resistance, improving biological compatibility, and reducing the leaching of metallic ions from the substrate material. However, there is limited research on the corrosion resistance of multilayer films (Ti, TiN, CrN) deposited using the cathode arc method. This technique offers high deposition rates due to elevated plasma ionization and ion energy levels. Therefore, coatings produced via

the cathodic arc method exhibit notable characteristics such as high hardness, strong adhesion to the substrate, high density, and uniformity. However, a drawback of this method is the increased roughness of the coating surface due to numerous macroparticles and pinholes, which can decrease the corrosion resistance of the coating surface. With this in mind, our study aims to evaluate the corrosion protection capabilities of multilayer coatings produced using cathode arc deposition on SS304 steel substrates. The ultimate goal is to determine the suitability of these coatings for medical applications.

2. EXPERIMENT

2.1 Coating deposition

TiN and CrN coatings were deposited using the cathodic arc deposition method with specially customized equipment. This apparatus includes a vacuum chamber with dimensions of $\Phi 500 \times 400$ mm, housing two arc heads with target dimensions of $\Phi 76$ mm $\times$ 20 mm. Additionally, the setup features one DC gun and one RF gun, both with target dimensions of $\Phi 76$ mm $\times$ 5 mm. High-purity titanium and chromium targets (99.95%) were utilized to deposit Ti, TiN, and CrN films. During the coating process, the substrate was heated to the requisite temperature using a resistive heating system positioned strategically at the bottom and center of the chamber.

Samples of 304 stainless steel, measuring 50x50x1.5 mm, were affixed to six rotating shafts operating at a speed of 8 revolutions per minute (rpm). These shafts were mounted on a rotating tray with a speed of 2 rpm. This configuration was designed to ensure a highly uniform coating formation on the substrate surface. The distances from the substrate to the shutter and target were 10 cm and 18 cm, respectively. To prevent overheating of the target and the chamber shell during the arc discharging process, a circulating cooling system was installed beneath the target and around the chamber wall (Fig. 1).

1. Grinding and Polishing: The 304 steel sample underwent a grinding process utilizing sandpaper with particle sizes ranging from 3 to 50 μm. These particle sizes corresponded to various types of sandpaper, including P120, P180, P240, P320, P400, P600, P800, P1000, P1200, P1500, P2000, and P2500, as per ISO 6344 standards. Following grinding, the sample was polished using a diamond paste (1 μm) in conjunction with a polishing cloth until a bright, mirror-like finish was achieved;

2. Chemical and ultrasonic cleaning: The sample was cleaned of residual grease using distilled water, alcohol, and acetone. It was then subjected to a 30-minute ultrasonic bath treatment, followed by another rinse cycle with distilled water, alcohol, and acetone;

3. Chamber preparation: The cleaned sample was positioned on a rotating table, maintaining a distance of 100 mm from the target's center. The chamber was then evacuated to a pressure of 9×10^{-6} torr;

4. Heating, plasma cleaning: The vacuum chamber was gradually heated to a temperature of 200°C using heating bars strategically placed along the chamber walls and in its middle. A 30-minute plasma cleaning process was initiated, involving the injection of argon gas into the chamber to attain a pressure of 200 mtorr, and applying a bias of -500V to the sample;

5. Coating deposition;

6. Cooling and venting: Upon completion of the deposition process, the sample underwent natural cooling within the chamber. Once the chamber's temperature descended below 70°C, the system was vented, and the sample was extracted from the chamber.

Tables 1 and 2 present the deposition parameters and coating structure for samples M1 to M4, each coated with a 2300 nm film. The composition of each sample is delineated as follows:

M1: Consists of a 50 nm Ti adhesion layer succeeded by a 2250 nm TiN layer. M2: Comprises 10 sublayers, each sublayer featuring a 30 nm Ti layer followed by a 200 nm TiN layer. M3: Involves 10 sublayers, with each sublayer encompassing a 30 nm Ti layer followed by a 200 nm CrN layer. M4: Composes of 10 sublayers, each sublayer including a 30 nm Ti layer, a 100 nm CrN layer, and a 100 nm TiN layer.
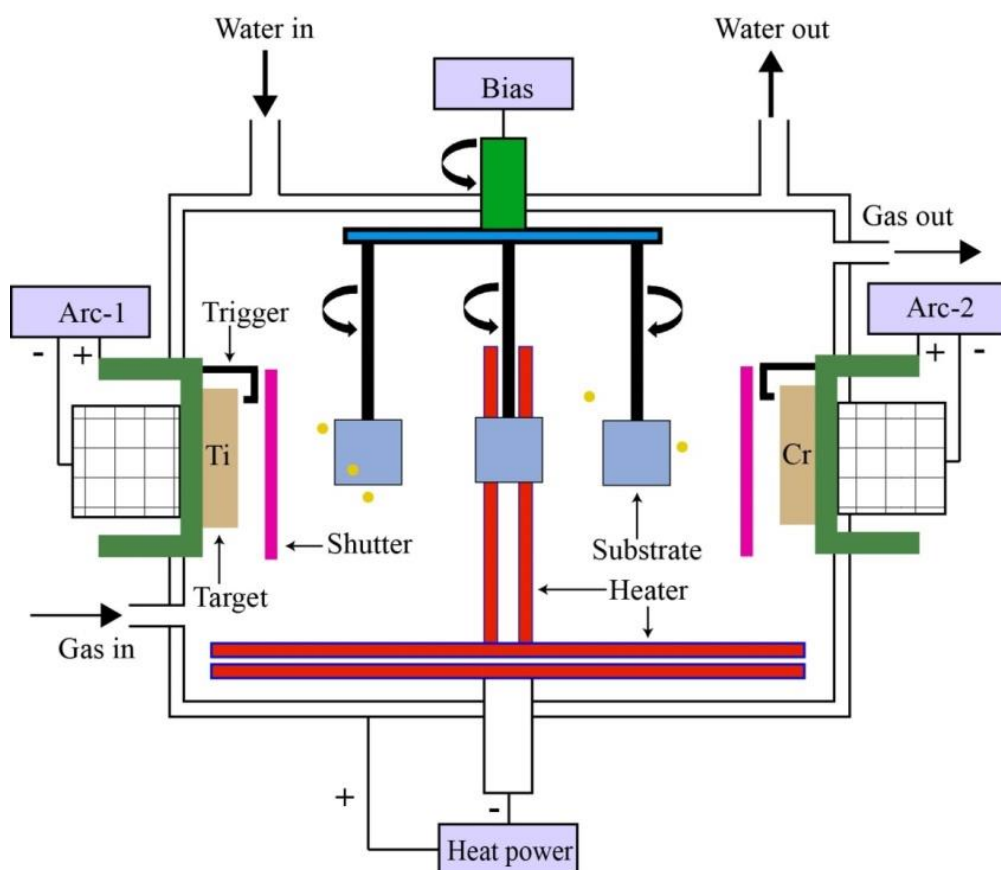
Fig. 1. Schematic of a cathodic arc evaporation system.

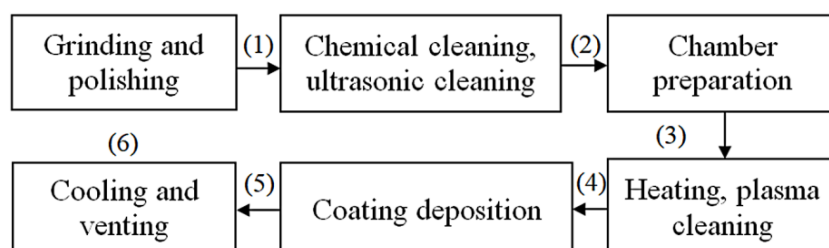The coating deposition process via the vacuum arc method is outlined in Fig. 2.

Fig. 2. Coating deposition process

Table 1. Deposition parameters.

Film	Target	Pressure, mtorr	Ar, sccm	N_2, sccm	Arc voltage, V	Arc current, A	Bias, V	Substrate temperature, ^{o}C
Ti	Ti (99,95%)	10	90	0	20	50	-60	200
TiN	Ti (99,95%)	10	10	90	20	50	-60	200
CrN	Cr (99,95%)	10	10	90	20	50	-60	200

Table 2. Structure of coatings.

Sample	Substrate material	Coating	Thickness (nm)	Number of layers	Total film thickness (nm)
M1	304	TiN/Ti	2250/50	1	2300
M2	304	TiN/Ti	200/30	10	2300
M3	304	CrN/Ti	200/30	10	2300
M4	304	TiN/CrN/Ti	100/100/30	10	2300

2.2 Film characterization

Film thickness was measured using an FE SEM S4800 microscope on the cross-section of the sample after grinding and polishing. Surface roughness assessment of the coated samples was performed employing the Laser Microscope OLS5100-SAF. The latter utilizes a non-contact 3D method, scanning an area of 128 μm × 128 μm to derive the average roughness value. To analyse the phase structure, X-ray diffraction was performed utilizing a PANalytical Empyrean X machine with CuKα radiation. The scanning speed (2θ/s) was set at 0.03º/s. To ascertain film adhesion to the substrate, adherence tests were executed in accordance with ISO 26443:2008 (E) guidelines, employing a Rockwell hardness tester and a Leica DMi8 microscope.

2.3 Electrochemical testing

Following coating deposition, samples with dimensions of Φ14x1.5 mm were laser-cut from the 50×50×1.5 mm specimens and subsequently cleaned with acetone in an ultrasonic bath for 15 minutes. The polarization curve was measured using the dynamic potential method at 25°C in a 3.5% NaCl solution, utilizing an Autolab Metrohm PGSTAT302N device equipped with a three-electrode system: the working electrode (WE) consisting of stainless steel coated with TiN and CrN films, the reference electrode (RE) comprising AgCl in saturated KCl, and the counter electrode (CE) made of platinum (Pt).

The corrosion resistance of coatings was studied with a scanning rate of 5 mV/s at an electrode polarization of ±1V, which was determined by the formula:

$$\eta = E - E_{corr} \qquad (1)$$

where E: electrode potential; E_{corr}: potential at which corrosion begins.

Prior to conducting the potentiodynamic polarization test, the samples were immersed in the solution for 300 seconds to establish the open-circuit potential. The corrosion potential (E_{corr}) and corrosion current (I_{corr}) were determined by Tafel polarization plot.

3. RESULTS AND DISCUSSION

The X-ray diffraction patterns of samples M1 to M4 are shown in Figure 3. These samples have an average thickness of 2300 nm, so X-rays penetrate through the coating to the SUS304 substrate. In addition to the typical TiN and CrN peaks, peaks of γ-Fe are visible at 43.473º, 50.674º, and 74.679 º (ICDD 00-023-0298). Sample M1 is coated with a film comprising a Ti adhesion layer (50 nm) and a TiN layer (2250 nm). The diffraction spectrum shows typical peaks for TiN at angles 36.806º, 42.612º (ICDD 00-006-0642: 36.806º; 42.612º; 61.982º; 74.200º), and the coating has a (111) preferential orientation. When interlaying the Ti layers with the TiN layer on sample M2, the peak intensities at the (111) and (200) faces were the same, indicating even growth in these two directions. The diffraction line at Ti(111) and Cr(111) appears broad, and the peak intensity of the multilayer is weaker than that of the single-layer coating. This is likely due to the presence of an amorphous phase, substantial grain refinement, and a high density of defects in the remaining crystalline structure [16.].

Sample M3 features a multilayer structure consisting of Ti (30 nm) and CrN (200 nm) sublayers. The spectrum displays peaks of CrN at angles 37.539º, 43.738º, and 63.541º (ICDD 00-011-0065) with a preferred orientation of (200). When depositing alternating Ti, CrN, and TiN layers on sample M4, the (111) face peaks of TiN and CrN were not recorded, and the film has a preferential (200) orientation. The shift in preferred orientation observed in the multilayer coating may be attributed to the preferred orientation of the CrN sublayer and the amorphization of the multilayer coating. The results show that multilayer structures lead to a shift in the preferred orientation from (111) to (200), contributing to increased coating hardness and elastic modulus [7,14,17,18]. This aligns with findings reported in previous studies [7,14,17,18]. Typically, TiN films with thicknesses in the tens of nanometers exhibit a (200) preferred orientation, while the (111) orientation becomes prevalent only when film thickness exceeds hundreds of nanometers. This transition can be attributed to the interplay between surface free energy and strain energy as the film thickness increases [14.].
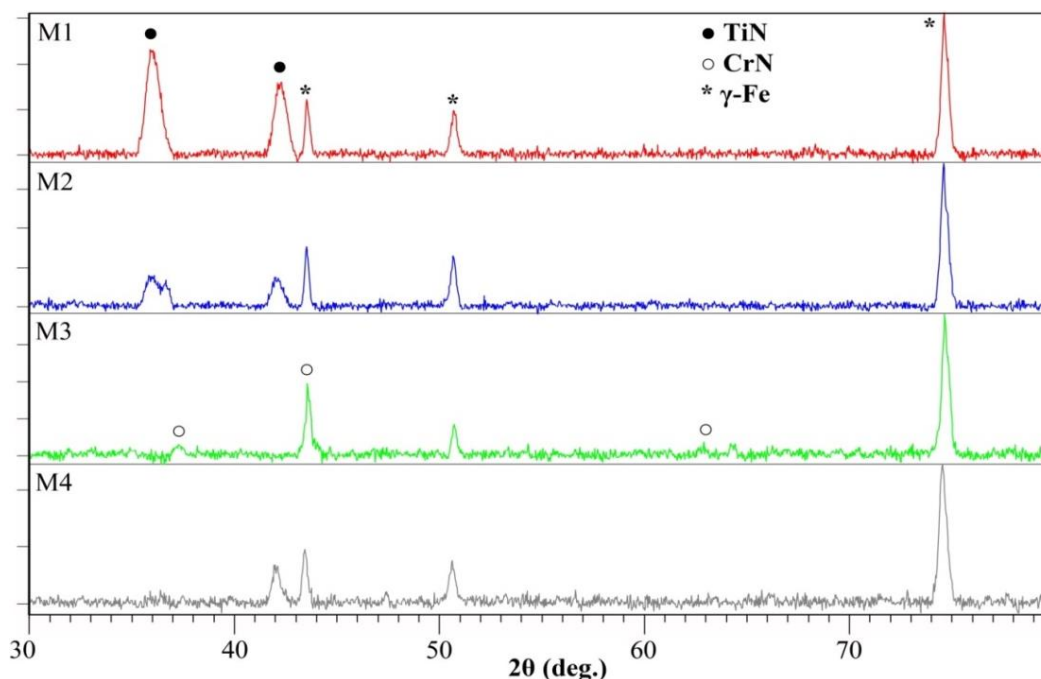
Fig. 3. X-ray diffraction spectra of the coatings.

Numerous macroparticles (peaks) and pinholes (valleys), ranging in size from 0.1 to 2 µm, were uniformly distributed on the sample surface, as illustrated in Fig. 4. The smallest number and size of macroparticles were observed in the sample coated with a single-layer TiN film (M1), whereas the largest was found in the sample coated with a multilayer TiN/CrN/Ti film (M4). The formation of these macroparticles is attributed to material "explosions" or the plasma pressure exerted within the cathode spot on the molten metal. Conversely, the valleys result from the detachment of these macroparticles from the coated surface, as discussed in a previous study [20.]. This phenomenon is inherent to the cathodic arc method and can only be mitigated using filters or adjusting deposition process parameters such as bias, gas ratio, and current.

Prior to deposition, the polished sample surface demonstrated a surface roughness of Sa = 0.009 µm. Post-deposition, the surface roughness escalated with the number of sublayers, ranging between 0.028 and 0.096 µm. The sample M1, featuring a single-layer TiN, showcased the lowest roughness at 0.028 µm. Conversely, samples M2 and M3, coated with two-component multilayer films of TiN/Ti and CrN/Ti, exhibited roughness values of 0.066 µm and 0.058 µm, respectively. The M4 sample, comprising a three-component TiN/CrN/Ti multilayer film, displayed the highest roughness at 0.096 µm (Fig. 5). This augmentation in roughness can be elucidated by the coating deposition mechanism. During the deposition of Ti, TiN, and CrN layers, the cycling power of Cr and Ti sources, coupled with variations in gas composition (N_2 and Ar), lead to an unstable material ejection process at the cathode spot resulting in the formation of numerous macroparticles within the coating.

Fig. 6 shows the cross-sectional structure of the samples. The monolayer coating applied to sample M1 exhibits a continuous columnar structure. This columnar structure is a characteristic feature commonly observed in coatings prepared through the cathode arc method [1]. It is typically associated with forming fine columnar crystallites during the growth process, which can lead to a high density of defects within the coating. In contrast, films deposited on samples M2 to M4 did not exhibit this columnar structure. The absence of continuous columnar growth in these samples can be attributed to Ti and CrN layers, which influence the film's structural development. This departure from the conventional columnar structure is a noteworthy outcome of the multi-component multilayer coatings used in these samples. The shift in coating architecture towards multilayer impacts the structural characteristics and yields advantages by enhancing the interface properties and creating effective barriers for protecting the substrate. This alteration in coating design contributes to improved performance, thus making it a significant aspect to consider in coating technology [2].
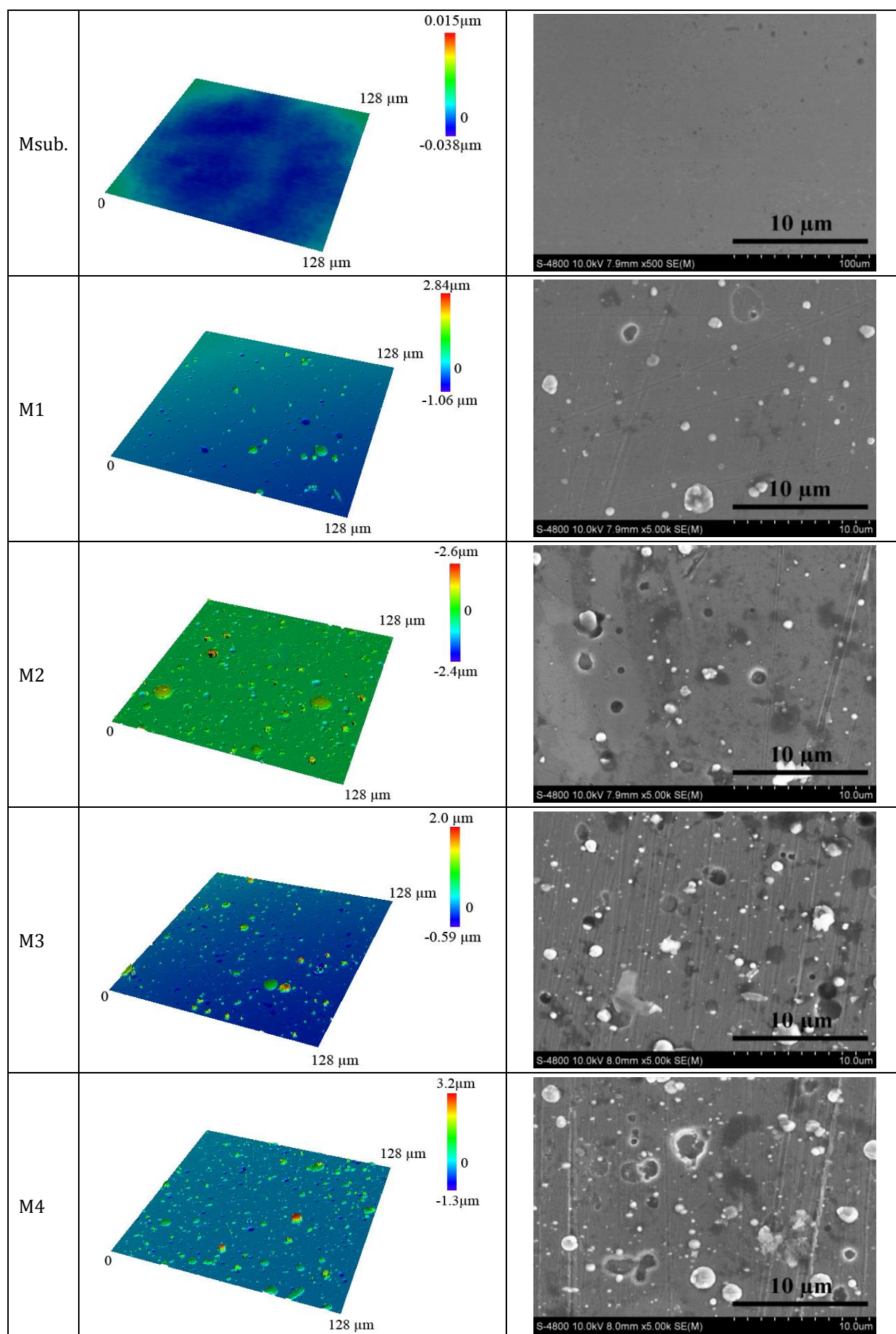
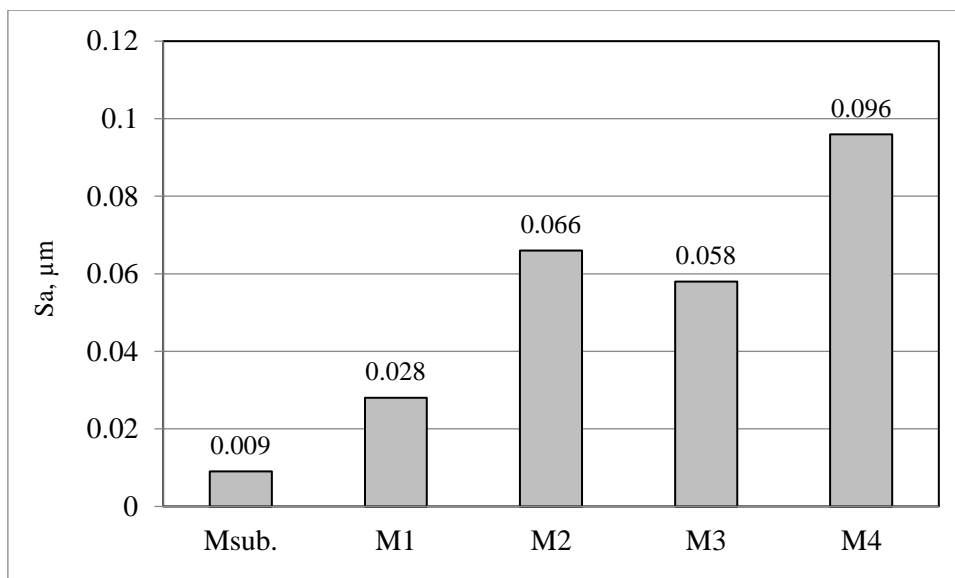**Fig. 4**. Sample surface after film deposition (FESEM and laser images).

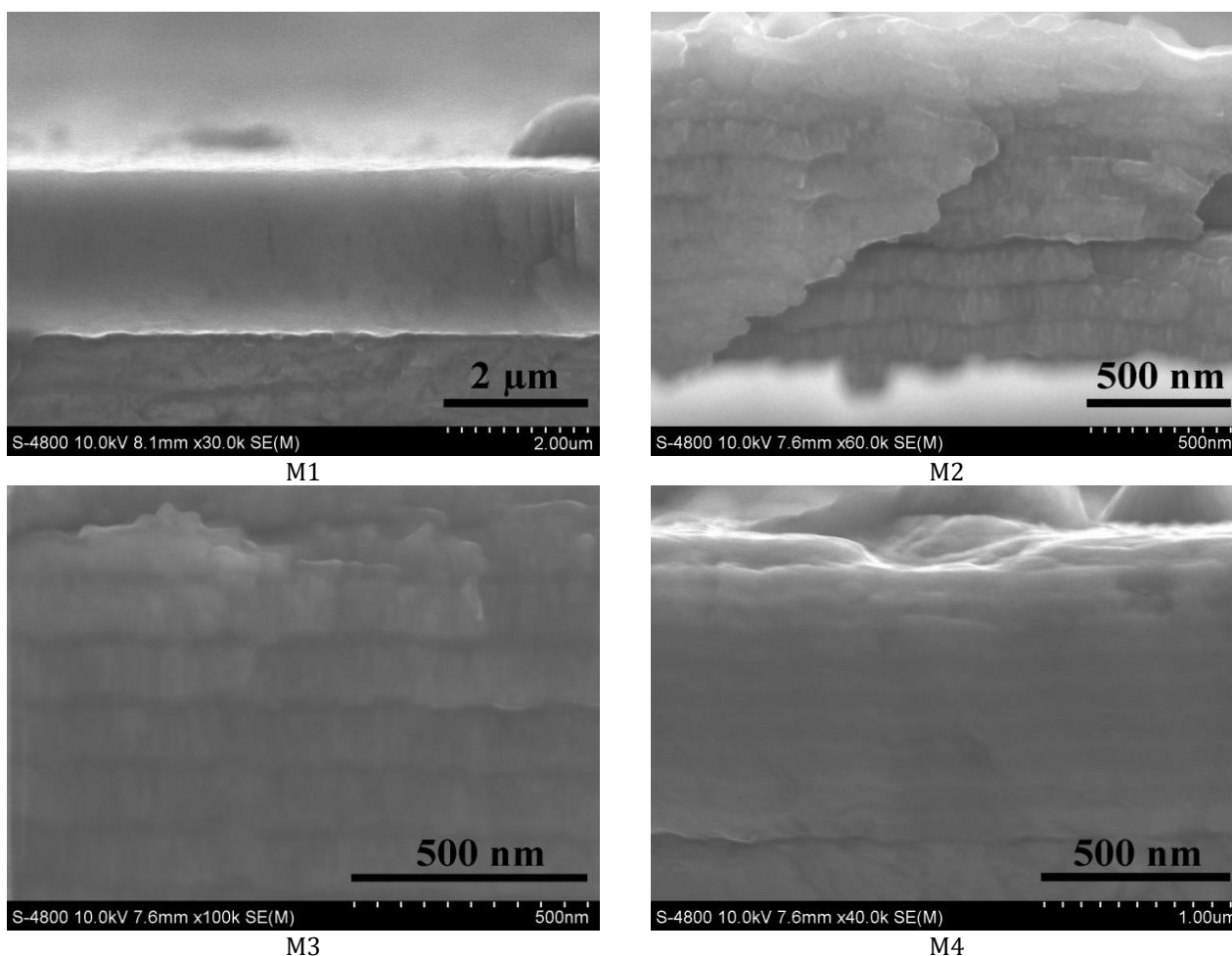**Fig. 5**. Surface roughness parameters of M1 after coating deposition.

Fig. 6. Coating cross-sectional structure after grinding and polishing (FESEM).

The adhesion test results were assessed in accordance with the ISO 26443:2008 standard. All samples, except for the monolayer sample M1, exhibited Class 0 adhesion (Fig. 7) without any cracks or peeling. The M1 sample (monolayer, 2300 nm) showed no adhesive or cohesive delamination around the indentation but had

some cracks in specific areas. According to ISO 26443:2008 (E), the adhesion grade of the M1 sample is categorized as Class 1. This finding indicates that the monolayer film, while meeting the ISO 26443:2008 (E) requirements, demonstrates relatively lower adhesion than the other samples. As mentioned earlier, the intermediate layers (Ti) serve as a buffer layer to help alleviate the stress within the coating caused by the high hardness of the TiN and CrN structure. Therefore, if the film is coated in a monolayer, increasing the thickness can easily lead to peeling [21].
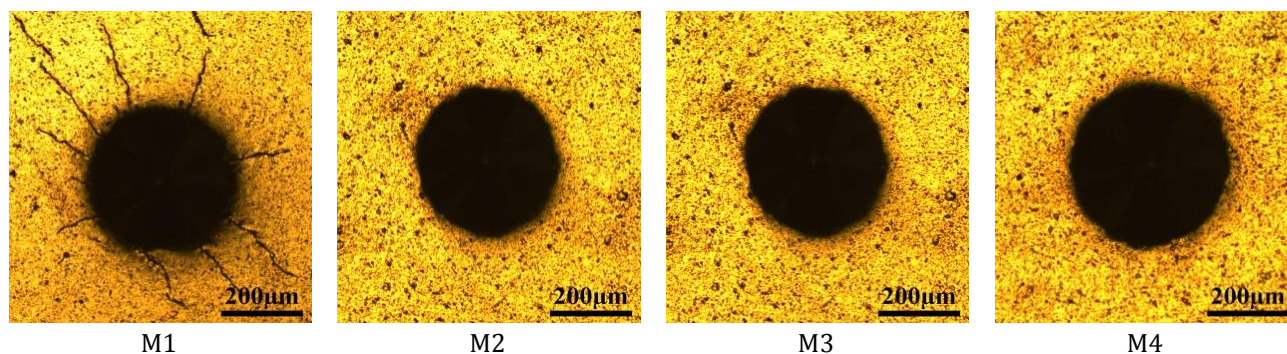
Fig. 7. Sample surface after adhesion test (50x magnification).

The results of the electrochemical corrosion measurement using the potentiodynamic polarization method are presented in Figure 8-11 and Table 3. The corrosion potential and corrosion current density were determined using the Tafel extrapolation technique as per ASTM G102-89 (2015) E1. Following the electrochemical test, an examination was conducted to identify pitting corrosion, characterized by the presence of spots or pits uniformly distributed across the test surface. Upon inspection of the coated samples, it was observed that pitting corrosion was only evident in sample M1, and in relatively limited quantities. In contrast, the remaining samples showed minimal to no discernible changes in their surface morphology (Fig. 9).

The analysis showed that the spots of corrosion, as shown in Fig. 9-10, had the greatest depth at their centers, gradually decreasing towards the edges. For sample M1, these corrosion spots tended to become deeper, while in the substrate sample, the corrosion spots tended to widen. Therefore, sample M1 had fewer corrosion spots, but each one was deeper (35 μm) compared to those observed in the substrate sample (32 μm). This difference in pitting corrosion behavior between the substrate and coated samples highlights the effectiveness of the multilayer coatings in providing corrosion resistance, warranting further investigation and analysis.

In samples M1 to M4, a slight increase in corrosion potential from -0.41 V (Msub.) to approximately -0.29 to -0.35 V (Table 3) was observed. The corrosion current decreased from 2.63×10^{-06} A (Msub.) to 1.49×10^{-07} A to 9.13×10^{-08} A, with a corresponding decline in current density from 3.50×10^{-06} A/cm^2 to 1.44×10^{-07} to 1.90×10^{-07} A/cm^2. The corrosion rate exhibited a reduction by a factor of 18-28 times compared to the uncoated sample (Msub.). The corrosion current density observed in our study aligns with the findings reported in a prior investigation [22], which involved potentiodynamic measurements of CrN and CrN/TiN coatings, deposited via the cathodic arc method, in a 3% NaCl solution. The recorded current density was 1.4×10^{-07} A/cm^2 for CrN and 1.7×10^{-07} A/cm^2 for CrN/TiN coatings. Both coatings exhibited corrosion potentials within the range of -0.515 V to -0.525 V, indicating a less noble electrode potential. Furthermore, Liu et al. [23] examined the electrochemical corrosion resistance of TiN and CrN coatings in a 0.5N NaCl solution. Notably, the corrosion potential of TiN and CrN multilayer films, applied to AISI 4135 steel through cathodic arc deposition, was determined to be -0.4 V and -0.45 V, respectively. The current density ranged from 3×10^{-06} A/cm^2 to 4×10^{-06} A/cm^2, suggesting comparatively lower corrosion resistance when contrasted with the values derived from this study.

Before	After	Before	After

M1 (TiN/Ti – monolayer coating)   M2 (TiN/Ti - multilayer coating)

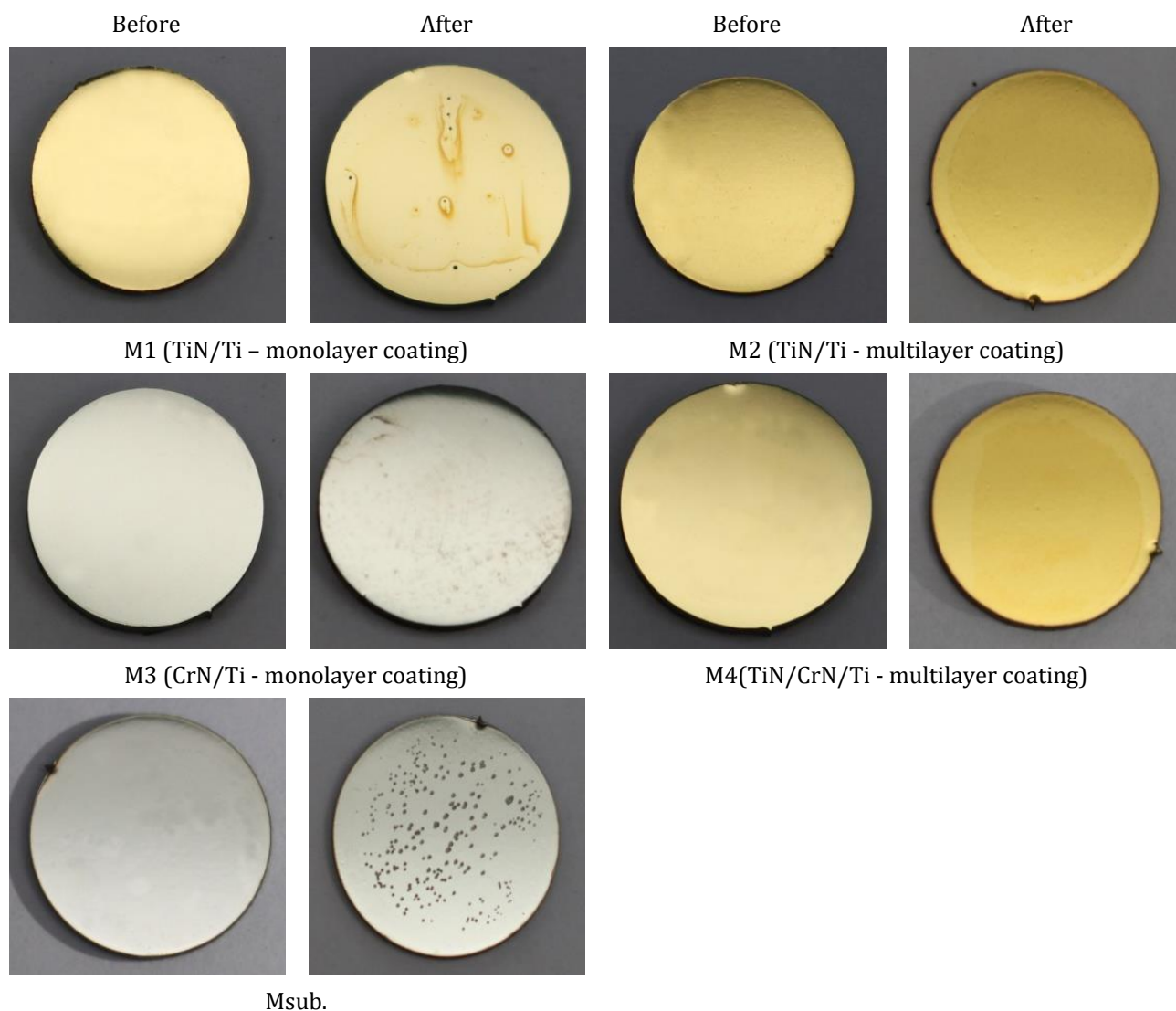M3 (CrN/Ti - monolayer coating)   M4(TiN/CrN/Ti - multilayer coating)

Msub.

**Fig. 8.** Sample surface before and after electrochemical test.

However, in other studies focusing on the production of nitride coatings through cathodic arc deposition, better corrosion potential, and corrosion density values have been reported. For instance, in the investigation conducted by He Tao et al. [24.] on Ti/TiN and Cr/CrN coatings deposited on a Ti-6Al-4V substrate, corrosion potentials were documented as -0.078 V and -0.026 V, while corrosion densities were reported as 1.48×10^{-6} A/cm^2 and 0.218×10^{-6} A/cm^2 for Ti/TiN and Cr/CrN coatings, respectively (3% NaCl). Similarly, in a separate study by Akeem et al. [25.], the corrosion potentials and corrosion densities of TiN and CrN coatings (3.5% NaCl) were identified as -0.196 V and -0.133 V, and 0.29×10^{-6} A/cm^2 and 1.24×10^{-6} A/cm^2, respectively. This highlights that technical parameters, equipment, and experimental setup significantly influence film quality beyond the coating structure and fabrication method. Therefore, to assess the corrosion resistance of materials, it is important to consider the increase in the corrosion current when the potential shifts in a positive direction [10,24]. For the substrate sample, the passive region occurs within the range of -0.3 to 0.3 V. In this range, a passive layer (Cr_2O_3) forms on the sample surface, preventing an increase in the corrosion current. However, as the corrosion potential increases, the passive layer is destroyed, leading to a rapid increase in the corrosion current. After testing, numerous spots resulting from pitting corrosion are visible on the uncoated sample surface.
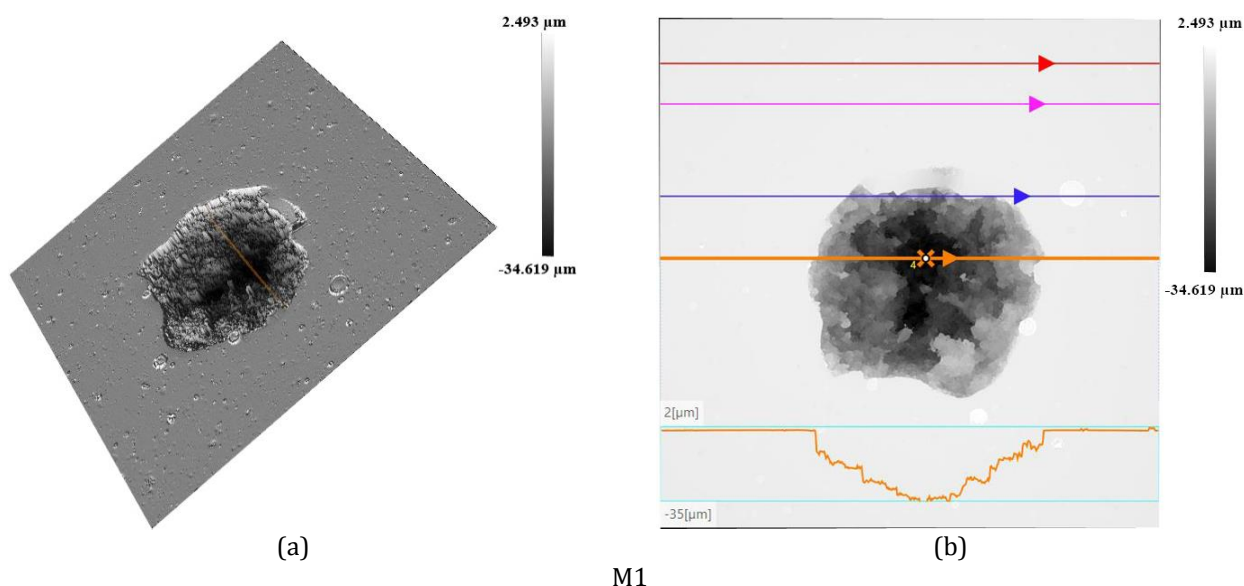
M1

Fig. 9. The surface of sample M1 after electrochemical testing, (a) 3D structure of corrosion points, (b) 2D structure of corrosion points with cross-section profile.
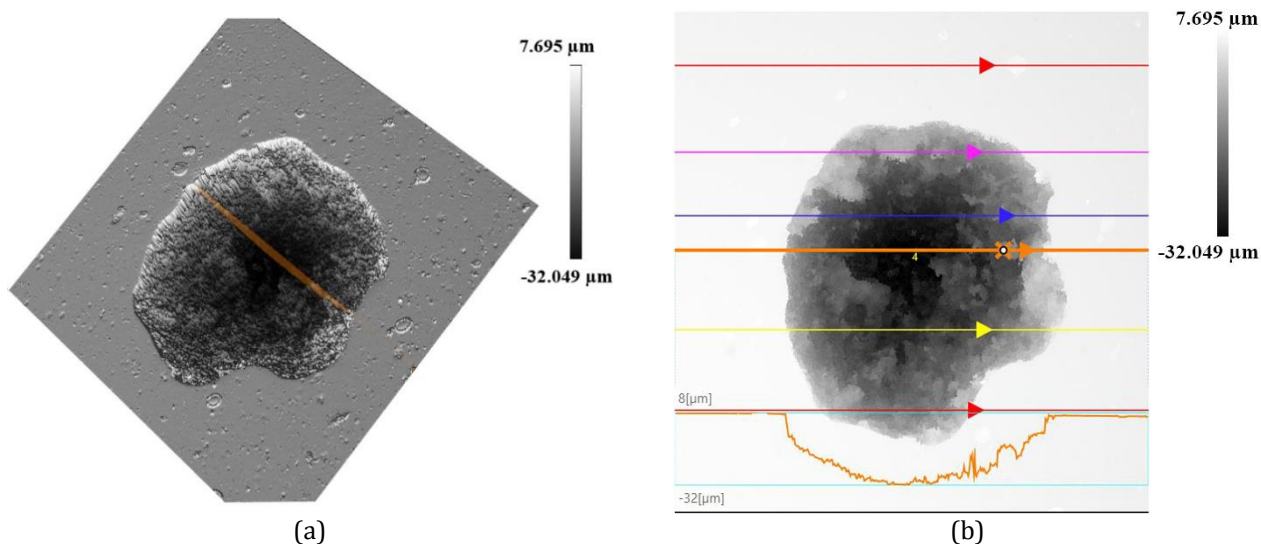
Msub.

Fig. 10. The surface of the substrate sample after the electrochemical test, (a) 3D structure of corrosion spot; (b) 2D structure of corrosion spot with cross-section profile.

The examination of Sample M1, a monolayer coating, revealed a limited passive range spanning from -0.2 V to 0 V, in contrast to the broader range of -0.3 V to 0.3 V observed in the substrate sample. Notably, the corrosion current of Sample M1 increased significantly as the corrosion potential exceeded 0 V. However, when the corrosion potential surpassed 0.4 V, the corrosion current of Sample M1 exhibited a comparatively slower rate of increase than that of the substrate sample. This behavior can be attributed to the formation of a columnar structure during the deposition process, characterized by numerous voids and gaps that facilitate the penetration of the electrolyte solution through the protective film, particularly when the coating thickness is inadequate. Once the electrolyte solution infiltrates the film, an electrochemical cell is established between the film and the substrate, thereby fostering corrosion. Consequently, beyond the potential breakdown point at 0 V, the Tafel line for Sample M1 adopts an almost vertical orientation. Notably, visible pitting corrosion sites became apparent on the surface of Sample M1, underscoring the intricate electrochemical dynamics at play and the susceptibility of the monolayer coating to localized corrosion phenomena.

The multilayer samples (M2, M3) demonstrated a passive range extending from -0.2 V to 0.3 V. Beyond this range, the corrosion current exhibited a prompt escalation, albeit at a relatively slower rate compared to the substrate sample (Fig. 11). Following the testing, the sample surfaces presented a darker hue. However, discernibly, no pitting corrosion spots were observed on the sample surfaces, as depicted in Fig. 8. The multilayer sample M4 exhibited the most extensive passive voltage range, spanning from -0.2 V to 0.6 V. Within this potential domain, the corrosion current displayed a gradual increase, with a sharp elevation observed only when the potential exceeded 0.8 V. Remarkably, post-testing, the sample's surface remained unaltered, devoid of any observable pitting corrosion. The findings of this study demonstrate better results than those of previous research by Liu and Paschoal [23,26]. According to Liu et al., the passive region for TiN and CrN films extends from -0.1V to 0.4V. Similarly, Paschoal et al. found that a TiN-coated film on stainless steel displayed a passivation zone ranging from -0.2V to 0.2V.

As specified in reference [27.], implant materials are required to surpass a breakdown potential of +600mV [SCE] when tested in a Phosphate-buffered saline solution with a salt content of approximately 1%. The observed onset of the breakdown potential at +800 mV during the assessment of sample M4 in a 3.5% NaCl solution denotes a favorable outcome, ensuring adequate corrosion resistance for the implant material. Titanium demonstrates superior antibacterial properties compared to commonly utilized metals in implant applications. The hierarchy of diminishing antibacterial activity across various materials is as follows: gold > titanium > cobalt > vanadium > aluminum > chromium > iron [28-31]. Furthermore, titanium presents a multitude of advantageous attributes, including a high level of biocompatibility, exceptional corrosion resistance, and robust osseointegration capabilities. Thus, using titanium with ceramic coatings such as TiN and CrN represents a viable strategy. The incorporation of alternating Ti layers between TiN and CrN layers serves a dual purpose: it acts as a preventive measure against the formation of columnar structures and minimizes stress between the TiN and CrN layers. This structural configuration fosters re-nucleation within the coatings, yielding numerous interfaces while concurrently reducing porosity. Consequently, this impedes the propagation of microcracks, prevents the formation of pinholes and pores, and obstructs electrolyte infiltration. As a result, the electrochemical corrosion process is restricted, consistent with findings outlined in prior research [1,2,10,32].
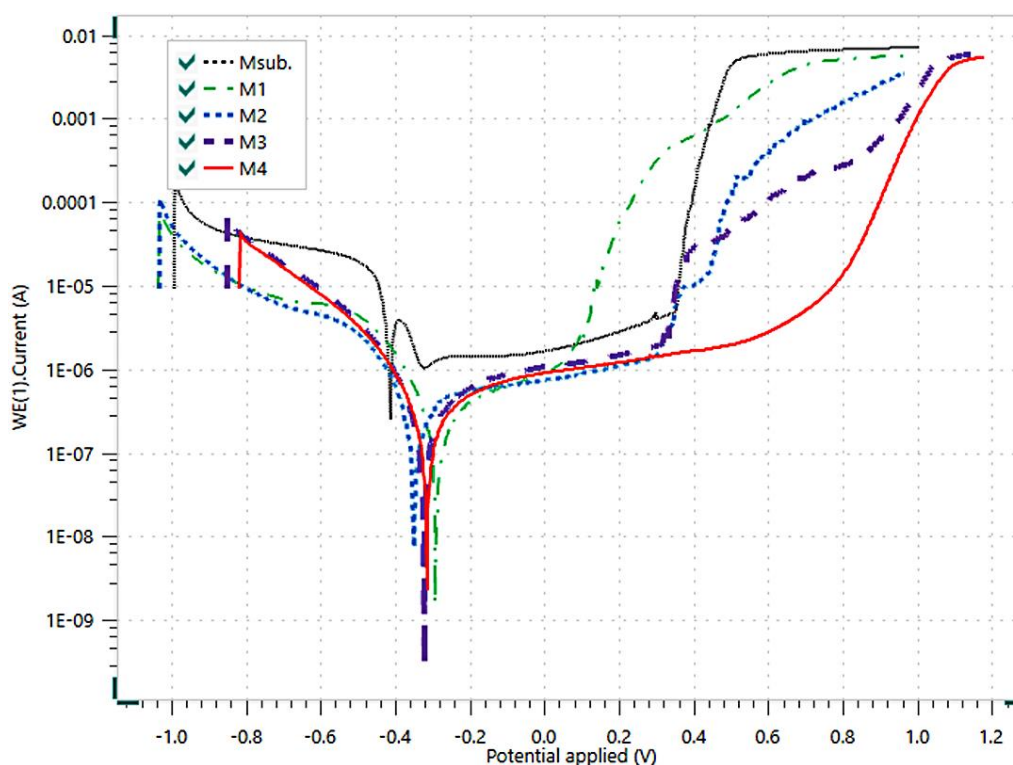

Fig. 11. Potentiodynamic polarization plots of substrate and coated samples.

Table 3. Electrochemical results from the potentiodynamic polarization curves of substrate and coated samples.

Sample	E_{corr}, (V)	j_{corr} (A/cm^2)	i_{corr} (A)	Polarization resistance (Ω)	Corrosion rate (mm/year)
Msub.	-0,41	$3,50 \times 10^{-06}$	$2,63 \times 10^{-06}$	6085	0,023056
M1	-0,29	$1,44 \times 10^{-07}$	$1,08 \times 10^{-07}$	201110	0,000898
M2	-0,35	$1,90 \times 10^{-07}$	$1,49 \times 10^{-07}$	164230	0,001266
M3	-0,32	$1,21 \times 10^{-07}$	$9,54 \times 10^{-08}$	183410	0,000789
M4	-0,312	$1,16 \times 10^{-07}$	$9,13 \times 10^{-08}$	206840	0,000764

4. CONCLUSION

- Monolayer TiN films have a smoother and more uniform surface with a roughness of 0.028 μm. In comparison, multilayer films have a relatively rougher surface, with the roughness of CrN/Ti and TiN/Ti coatings being 0.058 μm and 0.066 μm, respectively. Furthermore, the roughness of the TiN/CrN/Ti film is up to 0.096 μm.

- According to ISO 26443:2008 (E) standards, Monolayer film TiN/Ti with a thickness of 2.3 μm demonstrates lower adhesion compared to other films. This deficiency was attributed to the absence of Ti intermediate layers, which typically serve as buffer layers, effectively moderating stress within the film. Consequently, cracks can easily form when the film is subjected to external forces, emphasizing the importance of such intermediate layers for enhancing coating adhesion.

- The film exhibited a tendency to alter its preferred orientation from (111) to (200) in the presence of intermediate buffer layers composed of Ti. This phenomenon was consistently observed in TiN/Ti, CrN/Ti, and TiN/CrN/Ti multilayer coatings.

- The application of multilayer coatings has effectively expanded the passive range of corrosion resistance. Notably, the passive range for TiN/Ti and CrN/Ti coatings spans from -0.2 V to 0.3 V, while for TiN/CrN/Ti coatings, it extends from -0.2 V to 0.6 V. These ranges surpass the passive range of the SS304 substrate, which is -0.3 V to 0.3 V, as well as that of TiN monolayer coatings, which is -0.2 V to 0 V. This enhancement is primarily attributed to the capacity of multilayer structures to augment nucleation within the coatings, thereby impeding the diffusion of electrolyte solutions and retarding the electrochemical corrosion process. Multilayer structures based on TiN, CrN, and Ti offer distinct advantages in corrosion resistance compared to monolayer films. These structures exhibit promising potential for applications in medical devices such as screws and bone plates. However, comprehensive studies addressing their corrosion resistance and biocompatibility are imperative.

ORCID iDs

Vu Van Huy 0000-0002-7441-8050
Nikolai B. Rodionov 0000-0001-7505-4458
Valery A. Karpov 0009-0005-9696-6815
Ngo Thanh Binh 0000-0002-8623-3977
Doan Thanh Van 0000-0002-5529-7740
Nguyen Van Thanh 0000-0003-0619-8102

REFERENCES

[1.] N.S. Mansoor, A. Fattah-alhosseini, H. Elmkhah, A. Shishehian, "Comparison of the mechanical properties and electrochemical behavior of TiN and CrN single-layer and CrN/TiN multi-layer coatings deposited by PVD method on a dental alloy," *Mater. Res. Express*, vol. 6, p. 126433, Jan. 2019, doi: 10.1088/2053-1591/ab640d.

[2.] E. Lotfi-khojasteh, M. Sahebazamani, H. Elmkhah, M. Nouri, O. Imantalab, A. Fattah-alhosseini, "A study of the electrochemical and tribological properties of TiN/CrN nano-layer coating deposited on carburized-H13 hot-work steel by Arc-PVD technique," *Journal of Asian Ceramic Societies*, vol. 9, no. 1, pp. 270-282, Dec. 2020, doi: 10.1080/21870764.2020.1863577.

[3.] M.Z.B. Abdullah, M.A. Ahmad, A. N. Abdullah, et al, "Metal release of multilayer coatings by physical vapour deposition (PVD)," *Procedia Engineering*, vol. 148, pp. 254-260, Jun. 2016, doi: 10.1016/j.proeng.2016.06.612.

[4.] G.Lan, D. Yang, W. Chen, C. Wang, "Development and application of physical vapor deposited coatings for medical devices: A review," *Procedia CIRP*, vol. 89, pp. 250-262, Jan. 2020, doi: 10.1016/j.procir.2020.05.149.

[5.] B. Subramanian, K. Ashok, K. Subramanian, D. Sastikumar, G. Selvan, M. Jayachandran, "Evaluation of corrosion and wear resistance titanium nitride (TiN) coated on mild steel (MS) with brush plated nickel interlayer," *Surface Engineering*, vol. 25, pp. 490-495, Jul. 2009, doi: 10.1179/026708408X330621.

[6.] S.Calderon, C.F.A. Alves, N.K. Manninen, A. Cavaleiro, S. Carvalho, "Electrochemical corrosion of nano-structured magnetron-sputtered coatings," *Coatings*, vol. 9, pp. 682, Oct. 2019, doi: 10.3390/coatings9100682.

[7.] M. Ben Daia, P. Aubert, S. Labdi, C. Sant, F.A. Sadi, Ph. Houdy, J. L. Bozet, "Nanoindentation investigation of Ti/TiN multilayers films," *Journal of Applied Physics*, vol. 87, pp. 7753-7757, Jun. 2000, doi: 10.1063/1.373450.

[8.] N.D. Nam, M.J. Kim, D.S. Jo, J.G. Kim, D.H. Yoon, "Corrosion protection of Ti/TiN, Cr/TiN, Ti/CrN, and Cr/CrN multi-coatings in simulated proton exchange membrane fuel cell environment," *Thin Solid Films*, vol. 545, pp. 380-384, Oct. 2013, doi: 10.1016/j.tsf.2013.07.056.

[9.] Q. Yang, D.Y. Seo, L.R. Zhao, "Multilayered coatings with alternate pure Ti and TiN/CrN superlattice," *Surface and Coatings Technology*, vol. 177, pp. 204-208, Jan. 2004, doi: 10.1016/j.surfcoat.2003.09.033.

[10.] M. Herranen, U. Wiklund, J.O. Carlsson, S. Hogmark, "Corrosion behaviour of Ti/TiN multilayer coated tool steel," *Surface and Coatings Technology*, vol. 99, no. 1-2,, pp. 191-196, Feb. 1998, doi: 10.1016/S0257-8972(97)00525-2.

[11.] A. Dück, N. Gamer, W. Gesatzke, M. Griepentrog, W. Österle, M. Sahre, I. Urban, "Ti/TiN multilayer coatings: deposition technique, characterization and mechanical properties," *Surface and Coatings Technology*, vol. 142–144, pp. 579-584, Jul. 2001, doi: 10.1016/s0257-8972(01)01171-9.

[12.] Shanaghi Ali, Ghasemi Sajjad, Chu Paul, Sh. Ahangarani, Zhao Ying, "Effect of Ti interlayer on corrosion behavior of nanostructured Ti/TiN multilayer coating deposited on TiAl6V4," *Materials and Corrosion*, vol. 70, no. 1, p. 2113-22127, Jul. 2019, doi: 10.1002/maco.201910883.

[13.] T.D. Atmani, M. Gaceb, H. Aknouche, C. Nouveau, M.S. Bouamrene, "Parametric study of the mechanical properties of nanocrystalline TiN/CrN multilayer coatings with a special focus on the effect of coating thickness and substrate roughness," *Surfaces and Interfaces*, vol. 23, p. 101001, Apr. 2021, doi: 10.1016/j.surfin.2021.101001.

[14.] W.Du Jian, Li Chen, Jie Chen, L. Yue Jian, "Effects of additional oxygen on the structural, mechanical, thermal, and corrosive properties of TiN coatings," *Ceramics International*, vol. 48, no. 10, pp. 14432-14441, May 2022, doi: 10.1016/j.ceramint.2022.01.336.

[15.] A. Gilewicz, P. Chmielewska, D. Murzynski, E. Dobruchowska, B. Warcholinski, "Corrosion resistance of CrN and CrCN/CrN coatings deposited using cathodic arc evaporation in Ringer's and Hank's solutions," *Surface and Coatings Technology*, vol. 299, pp. 7-14, Aug. 2014, doi: 10.1016/j.surfcoat.2016.04.069.

[16.] M.Krasnowski, T. Kulik, "Amorphisation process during mechanical alloying of Al-Fe-Ti powders and crystallisation of the milling products," *Rev. Adv. Mater. Sci.*, vol. 18, pp. 393-397, Mar. 2008.

[17.] U. C. Oh, J. H. Je, "Effects of strain energy on the preferred orientation of TiN thin films," *Appl. Phys.*, vol. 74, pp. 1692-1696, Aug. 1996, doi: 10.1063/1.355297.

[18.] J. Pelleg, L. Z. Zevin, and S. Lungo, "Reactive-sputter-deposited TiN films on glass substrates," *Thin Solid Films*, vol. 197, pp. 117-128, Mar. 1991, doi: 10.1016/0040-6090(91)90225-M.

[19.] T. Q. Li; S. Noda; Y. Tsuji; T. Ohsawa; H. Komiyama, "Initial growth and texture formation during reactive magnetron sputtering of TiN on Si(111)," *Journal of Vacuum Science and Technology, Part A: Vacuum, Surfaces and Films*, vol 20, no. 3, pp. 583-588, May 2002, doi: 10.1116/1.1458944.

[20.] F. Sanchette, C. Ducros, T. Schmitt, P. Steyer, A. Billard, "Nanostructured hard coatings deposited by cathodic arc deposition: From concepts to applications," *Surface and Coatings Technology*, vol. 205, no. 23-24, pp. 5444-5453, Sep. 2011. doi: 10.1016/j.surfcoat.2011.06.015.

[21.] M. Nordin, M. Herranen, S. Hogmark, "Influence of lamellae thickness on the corrosion behaviour of multilayered PVD TiN/CrN coatings," *Thin Solid Films*, vol. 348, no. 1-2, pp. 202-209, Jul. 1999, doi: 10.1016/S0040-6090(99)00192-3.

[22.] J. Creus, H. Idrissi, H. Mazille, F. Sanchette, P. Jacquot, "Improvement of the corrosion resistance of CrN coated steel by an interlayer," *Surface and Coatings Technology*, vol. 107, no. 2–3, pp. 183-190, Sep. 1998, doi: 10.1016/S0257-8972(98)00646-X.

[23.] C. Liu, A. Leyland, Q. Bi, A Matthews, "Corrosion resistance of multi-layered plasma-assisted physical vapour deposition TiN and CrN coatings," *Surface and Coatings Technology*, vol. 141, no. 2–3, pp. 164-173, Jun. 2001, doi: 10.1016/S0257-8972(01)01267-1.

[24.] H. Tao, V. Zhylinski, A. Vereschaka, V. Chayeuski, H. Yuanming, F. Milovich, C. Sotova, A. Seleznev, O. Salychits. "Comparison of the Mechanical Properties and Corrosion Resistance of the Cr-CrN, Ti-TiN, Zr-ZrN, and Mo-MoN Coatings," *Coatings*, vol. 13, no. 4, pp. 750, Apr. 2023, doi: 10.3390/coatings13040750.

[25.] A.Y. Adesina, Z.M. Gasem, A. Madhan Kumar. "Corrosion Resistance Behavior of Single-Layer Cathodic Arc PVD Nitride-Base Coatings in 1M HCl and 3.5 pct NaCl Solutions," *Metall Mater Trans B*, vol. 48, pp. 1321–1332, 2017, doi.org/10.1007/s11663-016-0891-7.

[26.] P. André, C. Everaldo, C. Lauralice, D. S. Orivaldo, H. Domingos, M. Artur. "Metallic Biomaterials TiN-Coated: Corrosion Analysis and Biocompatibility," *Artificial organs*, vol. 27, no. 5, pp. 461-464, May 2003, doi: 10.1046/j.1525-1594.2003.07241.x.

[27.] R. Corbett, "Laboratory Corrosion Testing of Medical Implants," *Medical Device Materials - Proceedings of the Materials and Processes for Medical Devices Conference, Anaheim, California*, Sep. 2003.

[28.] M. Mohanty, S. Baby, K.V. Menon. "Spinal Fixation Device: A 6-Year Postimplantation Study," *Journal of Biomaterials Applications*, vol. 18, pp. 109-121, Oct. 2003.

[29.] M. Geetha, D. Durgalakshmi, R. Asokamani, "Biomedical Implants: Corrosion and its Prevention - A Review," *Recent Patents on Corrosion Science*, vol. 2, pp. 40-54, Jun. 2010. doi: 10.2174/1877610801002010040.

[30.] M. Abdulkareem, Z. Gbashi, B. Abdulhussein, M. Hanoon, A. Al-Amiery, and W. Al-Azzawi, "N-Methyl-2-(1-(5-methylthiophen-2-yl)ethylidene) hydrazinecarbothioamide as Corrosion Inhibitor for Mild Steel in HCl Solution: Weight Loss and DFT Investigations," *Journal of Materials and Engineering*, vol. 1, no. 4, pp. 164–173, Jan. 2023, doi: 10.61552/jme.2023.04.004.

[31.] C. W. Berry, T. J. Moore, J. A. Safar, C. A. Henry, M. J. Wagner, "Antibacterial activity of dental implant metals," *Implant Dent*, vol. 1, pp. 59-65, 1992. doi: 10.1097/00008505-199200110-00006.

[32.] I. A. Annon, K. K. Jlood, M. M. Hanoon, F. F. Sayyid, W. K. Al-Azzawi, and A. Al-Amiery, "Corrosion inhibition of mild steel in HCL solution using MPO: Experimental and theoretical insights," *Journal of Materials and Engineering*, vol. 2, no. 2, pp. 104–118, Jan. 2024, doi: 10.61552/jme.2024.02.002.